Nonlin. Processes Geophys. Discuss., 2, 969–987, 2015
www.nonlin-processes-geophys-discuss.net/2/969/2015/
doi:10.5194/npgd-2-969-2015

Nonlinear Processes
in Geophysics
Discussions
Open Access

Spectral characteristics of high latitude raw 40 MHz cosmic noise signals

C. M. Hall

Tromsø Geophysical Observatory, The Arctic University of Norway, Tromsø, Norway

Received: 05 May 2015 – Accepted: 02 June 2015 – Published: 07 July 2015

Correspondence to: C. M. Hall, (chris.hall@uit.no)

Published by Copernicus Publications on behalf of the European Geosciences Union & the American Geophysical Union.

Title Page
Abstract | Introduction
Conclusions | References
Tables | Figures
◀| | |▶
◀ | ▶
Back | Close
Full Screen / Esc
Printer-friendly Version
Interactive Discussion

Abstract

Cosmic noise at 40 MHz is measured at Ny-Ålesund (79° N, 12° E) using a relative ionospheric opacity meter ("riometer"). A riometer is normally used to determine the degree to which cosmic noise is absorbed by the intervening ionosphere, giving an indication of ionization of the atmosphere at altitudes lower than generally monitored by other instruments. The usual course is to determine a "quiet-day" variation, this representing the galactic noise signal itself in the absence of absorption; the current signal is then subtracted from this to arrive at absorption expressed in dB. By a variety of means and assumptions, it is thereafter possible to estimate electron density profiles in the very lowest reaches of the ionosphere. Here however, the entire signal, i.e. including the cosmic noise itself will be examined and spectral characteristics identified. It will be seen that distinct spectral subranges are evident which can, in turn be identified with non-Gaussian processes characterized by generalized Hurst exponents, α. Considering all periods greater than 1 h, $\alpha \approx 1.24$ – an indication of fractional Brownian motion, whereas for periods greater than 1 day $\alpha \approx 0.9$ – approximately pink noise and just in the domain of fractional Gaussian noise. The results are compared with other physical processes suggesting that *absorption* of cosmic noise is characterized by a generalized Hurst exponent ≈ 1.24 and thus non-persistent fractional Brownian motion, whereas *generation* of cosmic noise is characterized by a generalized Hurst exponent ≈ 1.

1 Introduction and instrumentation

The relative ionospheric opacity meter ("riometer") is a traditional instrument for measuring the degree to which cosmic noise is absorbed by the ionosphere (e.g. Little and Leinbach, 1959). By selecting a particular frequency for the riometer reception, it is possible to optimize the sensitivity to a particular altitude range and therefore how energetic the particles are that are causing the ionization. The means of analysing the signal from the riometer is to determine the “quiet day” variation and thereafter the degree of absorption caused by the intervening ionosphere. For a given radio wave frequency, the transmission, total reflection, partial reflection or absorption is indicated by the refractive index of the atmosphere. The refractive index of an ionized medium is in turn related to plasma parameters and the frequency of the radio wave in question by the Appleton–Hartree equation; this is thus a starting point for understanding the response of the riometer signal to varying degrees of particle precipitation (Hargreaves, 1979, 1992). Here, however the signal in its original form, as opposed to the derived absorption, will be examined, i.e. the cosmic noise as measured by a receiver at the Earth’s surface, since the object of this study is to investigate the spectrum of the signal itself including intermittency introduced by solar activity.

Data have been obtained from the recently established 40 MHz single beam riometer at Ny-Ålesund (79° N, 12° E), this being particularly undisturbed due to stringent restrictions on local activity such as use of radio and traffic. On the other hand, the location is well within the polar cap and the ionosphere is less disturbed by auroral activity than at, say, 70° N. The use of 40 MHz furthermore makes the instrument less sensitive to less energetic particles than, for example a 30 MHz instrument. Instruments such as the one used here are highly reliable and run unattended with minimal interruption. The riometer at Ny-Ålesund, manufactured by La Jolla Sciences of California, delivers signal strengths measured in mV every 2 s. Reception is via a 3-element crossed Yagi antenna having a half-power full-beamwidth of approximately 70°. Localized (with respect to the sky) sources of cosmic noise in the field of view as the Earth rotates are thus smoothed out by the wide antenna beam, and the undisturbed cosmic noise signal is therefore manifested by a smooth quasi-sinusoidal variation with period of one sidereal day (0.99726958 mean solar days). In general, the signal is characterized by this dominant variation. The amplitude of the sidereal diurnal variation varies with latitude, being zero at the pole (where the sky view is independent of time-of-day) and maximum at the equator. In addition, the quasi-sinusoidal signature is modulated by insolation that gives increased ionization during day and furthermore affects negative ion chemistry, a reduction in received cosmic noise occurring when the ionospheric D-region is sunlit. Although a seasonal effect at all latitudes, the degree of insolation changes more significantly at higher latitudes: in mid-winter, the lower D-region is not sunlit at all and vice versa in summer. These predictable periodic (deterministic) variations are discussed in the early reports by Forbush (1954 and 1958), which also contain pointers to similar work of the time, and an example of a more recent report is Behera et al. (2014).

As mentioned above, the idea of the riometer is to determine the absorption og cosmic noise due to perturbations in the intervening ionosphere due to space weather effects. These perturbations, in contrast to the largely deterministic quasi-diurnal and longer periods, end to be intra-diurnal and often of only ∼ hours duration, as for example, an auroral arc passes overhead (again, Hargreaves, 1979 and 1992, and references at the ends of the appropriate chapters). These variations are highly intermittent and can be expected to be as stochastic in nature as, for example, the solar activity that represents the underlying forcing. Finally, observations are typically influenced by local sources of disturbance such as nearby radio emissions and other radio frequency (RF) emissions from, for example, traffic. For the riometer used in this study, hourly calibration marks are also produced, but these are indeed hourly and therefore predicable. In addition, instrument noise is present to some degree, and the analogue to digital conversion is only 8-bit resulting in a degree of quantisation of the 2 s resolution readings. Although the riometer reacts instantaneously to ionospheric enhancement, a typical absorption event evolves over several measurements and therefore 1 min smoothing can be applied because in practice an observer would wait perhaps one minute to identify the event unambiguously. The entire dataset is portrayed in Fig. 1 after applying a 1 month running mean in order to illustrate the seasonal variation. Data from December 2013 to May 2015 are used in this study, again using the 40 MHz riometer at 70° N, 19° E. To illustrate the features described above, one day of data (20 September 2014) are plotted in Fig. 2. The smooth line is a 10 min running mean of the underlying data, in which the 8-bit quantisation can be seen together with the hourly calibration (normally negative) spikes. The sidereal-day variation is the obvious overall feature, and when successive calendar days are plotted, the phase is seen to migrate to the left by approximately 4 min per day. Despite the smoothing, the absorption events at 1330 and 1500 are well identified. The first absorption event is short-lived (∼ 1 h) whereas the second event is longer, evidently continuing through the rest of the day. It should be stressed that these individual events per se are not the subject of this study, Figs. 1 and 2 merely illustrate the long-and short-term variations in the dataset. In the following sections, the spectral characteristics of the entire dataset will be examined and discussed, thus including the deterministic periodicities and the collection of intermittent absorption events. As a major feature of the discussion, the non-Gaussian nature of the distribution of the stochastic part of the signal will be addressed.

A significant problem in the study of physical systems is the identification of coupling between processes, what are causes and what are true effects. An evolving approach is to examine the stochastic nature of the signals from different processes because noise present in a cause will presumably be also present in resulting effects. The noise signatures may not be unambiguous of course, so any apparent coupling must be treated with care. Although gaining popularity, the principle was introduced by, inter alios, Hurst (1951), Mandelbrot (1983), Grassberger and Procaccia (1983) and Koscielny-Bunde et al. (1998) and later explored by (e.g.) Eichner et al. (2003), Lennartz and Bunde (2009), Kantelhardt et al. (2006), Rypdal and Rypdal (2011), Hall (2014a, b). The concepts of fractional Gaussian noise (fGn) and fractional Brownian motion (fBm) have been proposed by Mandelbrot and van Ness (1968), and the Hurst exponent, H, by Hurst, (1951) all to help quantify self-affinity of stochastic components of time-series. For fBm, successive increments are correlated resulting from the time-series being non-stationary and with temporally changing variance; for fGn, the time-series is stationary and expectation value and variance are time-invariant. The Hurst exponent is not able to differentiate between these processes, however, and here the approach of Kantelhardt et al. (2006) is adopted to derive rather the *generalized Hurst* *exponent*, α. The two exponents are related: for fGn, $H = \alpha$ and for fBm, $H = \alpha - 1$. The exponent α unambiguously characterizes the process as fBm ($\alpha > 1$), or fGn ($0 < \alpha < 1$). Furthermore, a process can be described as anti-persistent when an increment is likely to be followed by one in the reverse direction: for fGn, $0 < \alpha < 0.5$ and for fBm $1 < \alpha < 1.5$. On the other hand, persistent is when an increment is more likely to be followed by one in the same direction: for fGn, $0.5 < \alpha < 1.9$ and for fBm $\alpha > 1.5$. The case $\alpha = 1.5$ indicates the (well-known) special case of Brownian motion. One method to determine α is first to find the scaling exponent β of the power spectrum $S(f)$, f being frequency:

$$S(f) \propto |f|^{-\beta} \tag{1}$$

Thereafter, the *generalized Hurst exponent, α* is related to β by

$$\alpha = (\beta + 1)/2 \tag{2}$$

the derivation of which can be found in, e.g., Hartmann et al. (2013), and Delignieres et al. (2006), and references therein.

Using the approach of Hall (2014a, b), the stochastic component of the time-series is isolated from the slowly evolving (deterministic) component. Here, a smoothed time-series will be subtracted from the original and the residual will be deemed stochastic, as will be demonstrated in the following section. From the stochastic (noise) component, the probability density function (PDF) of the data is obtained and thereafter quantile-quantile (Q–Q) analyses (Wilk and Gnanadesikan, 1968) performed. To produce Q–Q plots, quantiles of the distribution of signal noise are plotted against corresponding quantiles for hypothesized distributions exhibiting the same mean and standard deviation. A visual inspection of the PDF can indicate if the signal's noise distribution is Gaussian or otherwise. From an inspection of the Q–Q plots the degree to which the signal's noise distribution agrees with that hypothesized: a straight line indicating agreement.

In this study, the goal is to investigate the spectrum of the cosmic noise data in its entirety, encompassing variations at all timescales. The starting point is not, therefore a derived stochastic component. Furthermore, experimental data, including gaps due to instrument failure are almost invariably irregularly sampled and therefore the Lomb–Scargle periodogram analysis (Press and Rybicki, 1989) will be used rather than a traditional Fourier transform. Fougère (1985) and Eke et al. (2000) propose preconditioning of the time series by applying a parabolic window, thereafter bridge detrending using the first and last points in the series, and then a final frequency selection before identifying subranges exhibiting linear dependence in lo-log space. This last step however will be omitted in order to retain as much spectral information as possible, at least initially.

It should be mentioned that several approaches are available for estimating H or α, the most popular perhaps being the detrended fluctuation analysis (DFA) (Peng et al., 1993). Physicists in general are familiar with spectral analyses, this being the focus here. For reference, commonly used methods including spectral analysis (SA) have been described by Delignieres et al. (2006), Hartmann et al. (2013) and Heneghan and McDarby (2000).

2 Analyses

As described in the previous section, an approximation to the stochastic component of the cosmic noise signal is extracted from the complete dataset. Which timescales contain deterministic signals is open to discussion; since perturbations resulting from solar-terrestrial interaction can recur over periods of days (such as some polar cap absorption events), the time series shown in Fig. 1. has been deemed deterministic. This is then subtracted from the original and the residual deemed largely stochastic. A corresponding method was employed by Hall (2014b). As will be seen, spectral analysis identifies individual periodicities remaining in the (supposedly) stochastic residual, these showing up as narrow spikes. Due to the large number of data points and therefore frequencies in the spectrum, these spikes impose insignificant influence when determining the spectral slope. A disadvantage with DFA is that such periodicities are generally *not* easily distinguishable.

The probability density function (distribution) of the stochastic component is determined and shown in Fig. 3. The distribution is centred on zero resulting from subtraction of the deterministic component. A Gaussian distribution is fitted that fails to reproduce the narrowness of the distribution of the observation at half height. By using a different parameterization of the distribution width than half-maximum full-width, viz. $1/e$ of maximum, a wider Cauchy distribution is modelled that fits the data better (suggested by Hall, 2014b). Qualitatively the Cauchy model describes the distribution considerably better than the Gaussian, but all the same, a heavy "shoulder" is evident for reduced values of cosmic noise. The centre and right panels of Fig. 3. show the quantile-quantile (Q–Q) portrayals – vs. Gaussian (centre) and vs. Cauchy (right). The means of interpreting such Q–Q plots are described by Chambers et al. (1963). Departures from linearity (in the central regions of the plots) indicate heavy shoulders at both sides (sometimes referred to as long tails) of the distribution relative to the model. It can be seen that the Cauchy model approaches the shoulders in the distribution of the measurement somewhat better than the Gaussian. In fact, a Cauchy model will always represent the long tails in a distribution better than a Gaussian as can be seen in the left-hand panel. As explained by Sato (1999), a Cauchy process is be defined as Brownian motion subordinated to a process associated with a Lévy distribution. The portrayals in Fig. 3. point to a Lévy process being the best description of the stochastic component rather than Gaussian noise.

For determination of power spectral density, the entire original dataset is employed, such that all conceivable fluctuations are included. There are therefore no a priori assumptions as to which fluctuations are truly non-chaotic. The exception is the sidereal periodicity, but as stated earlier, this represents but one narrow spike in the spectrum compared with all other frequencies present and does not influence the identification of subranges exhibiting scaling and subsequent determination of exponents β. Prior to spectral analysis, the data are preconditioned by applying a parabolic window and then bridge detrending using the first and last points as described in the previous section. Thereafter, the Lomb–Scargle periodogram analysis is applied, again as explained earlier. The result is shown in Fig. 4. In reality, a considerable amount of (approximately) white noise results at periods shorter than 1 min and these are associated with instrumental noise and quantization of measurements due to the use of an 8 bit analogue-to-digital converter. The first indication of this instrumental noise is seen at the very right-hand end of the plot, and the remainder is omitted in order not to detract from the characteristics of the received signal itself. Meaningful timescales are indicated on the figure for the convenience of the reader: 1 min, 1 h and 1 day, the last being the sidereal day. The scaling is quite evident, although delineation of separate subranges is somewhat subjective. Since experience shows that, for example, auroral activity in the field of view of such instruments as the riometer (depending of course on the antenna type) last from typically minutes to hours, linear fits to the log-log spectrum have been performed for all periods greater than 1 min, 1 h and 1 sidereal day. Due to the high density of points at high frequencies, the >1 min period sub-range is heavily weighted towards 1 h to 1 min etc. The respective fits are superimposed on the plot. For periods <1 min, $\beta = 0.72 \pm 0.001$; for periods <1 h, $\beta = 1.48 \pm 0.006$; for periods <1 day, $\beta = 0.87 \pm 0.035$.

3 Discussion

The first characteristic to note is that for all variability in 30 MHz cosmic noise at timescales shorter than 1 month, the probability density function is not well represented by a Gaussian distribution. The attempt to fit a Cauchy distribution defining the width being at $1/e$ as opposed to $1/2$ maximum succeeded in matching the heaviness in the tails of the distribution, but not the narrowness on the peak. By definition, the Cauchy distribution is symmetric, and therefore while the model represents the heavy tail for positive values, the presence of the negative shoulder is conveniently accentuated. It should be remembered, however, that the approach is rather simplistic. Qualitatively the distribution is reminiscent of a Lévy process (which is also represented by a Cauchy distribution) but no attempt will be made to sub-classify this further here, the method being fraught with pitfalls (e.g. see Rypdal and Rypdal, 2010). Examining the Q–Q plots, the heavy-tailed distribution is characterized by the downward trend at the left-hand ends and upward trend at the right-hand ends of both Gaussian and Cauchy versions. The overall upward curvature in the Cauchy plot indicates a degree of skewness due to the shoulder. Lack of discontinuities indicate lack of bimodal (or multimodal) distributions. Recalling that the above analyses have been performed on the residual after subtracting the smoothed data from the original observation, the negative values in the distribution are associated with reductions in the original signal. Thus, the shoulder in the distribution and the evidence for skewness in the Q–Q plots are readily explained by intra-day absorption events, their intermittent signature contributing to, if not responsible for, the non-Gaussian probability density function.

Turning to the spectral analysis, there is an indication that 3 subranges are present in the spectrum. Timescales associated with auroral activity which, in turn correspond to enhanced electron densities in the ionospheric D region, are typically minutes to hours. One can envisage an auroral arc moving across the sky; although this will be in one position for a short time interval, it will be in the riometer antenna beam for much longer. The response of a ground-based magnetometer is similar as described by Hall (2014b), although current systems causing perturbations in the geomagnetic field typically occur at higher altitude than ionisation modulating cosmic noise at 40 MHz. It can therefore be hypothesized that the scaling exponent for periods > 1 h is associated with absorption events, and, at that, caused by high-energy precipitation, since the riometer is within the auroral oval and receives at 40 MHz. If the reader is unfamiliar with ionospheric physics, clarification can be obtained by reading appropriate chapters in (e.g.) Hargreaves (1979 and 1992) and the recent study by Kellerman et al. (2014) contains an exhaustive source of references. For periods > 1 day, variation of the signal is largely predicable from the geometry of the rotation of the observation point relative to the galaxy.

Title Page
Abstract Introduction
Conclusions References
Tables Figures
◀| |▶
◀ ▶
Back Close
Full Screen / Esc
Printer-friendly Version
Interactive Discussion

Nevertheless, solar activity responsible for polar cap absorption events can persist for consecutive days and the associated absorption is modulated by the Earth's rotation and compounded by ion chemistry. For the shortest timescales before the onset of the approximately white instrumental noise described earlier, it is somewhat unclear as to which processes are responsible for the less steep ($\sim$ unity) spectral exponent. It will be instructive to convert the spectral exponents (β) to generalized Hurst exponents (α) for comparison with similar analyses of potentially related solar and terrestrial metrics. For periods > 1 day, $\alpha = 0.94 \pm 0.04$; for periods > 1 h, $\alpha = 1.24 \pm 0.01$; for periods > 1 min, $\alpha = 0.86 \pm 0.00$. These values indicate that the $>$ hour subrange is characterised by non-persistent fractional Brownian motion (fBm) whereas the other subranges either side are characterized by (marginally) fractional Gaussian noise (fGn) or approximately $1/f$ fluctuations. For longer period variability the hypothesis that the spectral exponent is relatively unrelated to high energy particle precipitation is supported by good agreement with the results of Canal et al. (2012) who report $1/f$ scaling for low energy secondary cosmic ray flux at low frequencies. On the other hand, Canal et al. (2012) find sunspot variation for periods less than 1 month to be characterized by $\beta \approx 1.4$, or $\alpha \approx 1.2$. This is the same as the $>$ hours value reported here (viz. 1.24). Solar activity can by parameterized by a number of metrics including sunspot number and of course is the ultimate cause of ionospheric enhancements that give rise to riometer response at these timescales. It is interesting to note that a plethora of investigations of scaling in parameters related to auroral activity in the auroral oval (i.e. on average equatorward of 79° N indicate, although not exclusively, generalized Hurst exponents somewhat larger than reported here and suggestive of persistent fBm. One example is an analysis of Disturbance storm time (Dst) index by Balasis et al. (2006), reporting scaling in the range (5 days–2 h) with α between ~ 1.4 and ~ 1.6. For the geomagnetic field in the auroral oval, Hall (2014b) similarly reports α between ~ 1.39 and ~ 1.54 and Hamid et al. (2009) assert that for active days the geomagnetic activity scales with $\alpha > 1.5$. In summary, three spectral subranges can be identified apart from the white noise deemed instrumental: a short timescale regime of the order of minutes to hours, exhibiting $1/f$ scaling, an intra-day timescale with a spectral slope of ~ 1.4, and finally a longer timescale regime also exhibiting $1/f$ scaling. For the first of these it is difficult to identify a specific underlying physical process; for the second, similarity with intra day variability in the geomagnetic field and with solar disturbances suggests solar origins and therefore cosmic noise absorption: the last has similarities with slow fluctuations in independent determinations of cosmic ray intensity therefore confirming origins in cosmic ray sources.

4 Conclusions

Cosmic noise signal at 30 MHz has been recorded at 79° N, 12° E within the polar cap, providing, for this study, a time-series of approximately 18 months at 2 s resolution. Examinations of probability density function and quantile-quantile plots reveal that the data can hardly described by a Gaussian distribution, and that a Cauchy model fits better, thus suggesting an underlying Lévy process of some form. The power spectral density exhibits spectral subranges with differing scaling properties. The minute-to-hour fluctuations are characterized by $1/f$ scaling, the physical meaning of which is difficult to identify. The hour-to-day fluctuations are characterized by a spectral exponent of ~ 1.4 corresponding to a generalized Hurst exponent of 1.24 suggestive of anti-persistent fractional Brownian motion; these are associated with absorption-reduction of cosmic noise signal due to the intervening ionosphere in turn modulated by solar activity. Fluctuations longer than $\sim$ day timescales are characterized by $1/f$ scaling and comparison with other studies supports a hypothesis that cosmic noise intensity itself – i.e. independent of the intervening ionosphere is responsible. Key products transpire from this study: (a) that signal variation with scales of $\sim$ hours to days contains information on cosmic noise absorption and are therefore relevant for space weather considerations, whereas timescales shorter and longer contain information relating to other physical processes, (b) underlying physical processes can be identified in riometer data by classification in terms of the generalized Hurst exponent.

Title Page
Abstract | Introduction
Conclusions | References
Tables | Figures
◀| |▶
◀ ▶
Back | Close
Full Screen / Esc
Printer-friendly Version
Interactive Discussion

Subsequent investigation could include examination of cosmic noise signals at both 30 and 40 MHz from receivers within, under and outside the auroral oval, together with corresponding magnetometer analyses. Such results would be valuable to substantiate the aforementioned hypotheses but more importantly to establish dependence of the spectral characteristic on geomagnetic latitude and energies of precipitating particles.

Acknowledgements. Data from the Ny-Ålesund station can be obtained via Tromsø Geophysical Observatory.

References

Balasis, G., Daglis, I. A., Kapiris, P., Mandea, M., Vassiliadis, D., and Eftaxias, K.: From pre-storm activity to magnetic storms: a transition described in terms of fractal dynamics, Ann. Geophys., 24, 3557–3567, doi:10.5194/angeo-24-3557-2006, 2006.

Behera, J. K., Sinha, A. K., Singh, A. K., Rawat, R., Vichare, G., Dhar, A., Pathan, B. M., Nair, K. U., Selvaraj, C., and Elango, P.: First results from imaging riometer installed at Indian Antarctic station Maitri, J. Earth Syst. Sci., 123, 593–602, 2014.

Chambers, J. M., Cleveland, W. S., Kleiner, B., and Tukey, P. A.: Graphical Methods for Data Analysis, Duxbury Press, Boston, Massachusetts, 395 pp., 1963.

Canal, C. A. G., Hojvat, C., and Tarutina, T,: Scaler mode of the Auger Observatory and sunspots, Astrophys. J. Suppl., 202, 16–22, doi:10.1088/0067-0049/202/2/16, 2012.

Delignieres, D., Ramdani, S., Lemoine, L., Torre, K., Fortes, M., and Ninot, G.: Fractal analyses for “short” time series: a re-assessment of classical methods, J. Math. Psychol., 50, 525–544, 2006.

Eichner, J. F., Koscielny-Bunde, E., Bunde, A., Havlin, S., and Schnellnhuber, H.-J.: Power-law persistence and trends in the atmosphere: a detailed study of long temperature records, Phys. Rev. E, 68, 046133, doi:10.1103/PhysRevE.68.046133, 2003.

Eke, A. H., Hermán, P., Bassingthwaighte, J. B., Raymond, G. M., Percival, D. B., Cannon, M., Balla, I., and Ikrényi, C.: Physiological time series: distinguishing fractal noises from motions, Pflug. Arch. Eur. J. Phy., 439, 403–415, 2000.

Forbush, S. E.: World-wide cosmic-ray variations 1937–1952, J. Geophys. Res., 59, 525–542, 1954.

Forbush, S. E.: Cosmic-ray intensity variations during two solar cycles, J. Geophys. Res., 63(4), 651–669, 1958.

Fougère, P. F.: On the accuracy of spectrum analysis of red noise processes using maximum entropy and periodograms methods: simulation studies and application to geographical data, J. Geophys. Res., 90, 4355–4366, doi:10.1029/JA090iA05p04355, 1985.

Grassberger, P. and Procaccia, I.: Measuring the strangeness of strange attractors, Physica D, 9, 189–208, 1983.

Hall, C. M.: Complexity signatures for short time scales in the atmosphere above Adventdalen, Svalbard, J. Geophys. Res.-Atmos., 119, 652–662, doi:10.1002/2013JD020988, 2014a.

Hall, C. M.: Complexity signatures in the geomagnetic H component recorded by the Tromsø magnetometer (70° N, 19° E) over the last quarter of a century, Nonlin. Processes Geophys., 21, 1051–1058, doi:10.5194/npg-21-1051-2014, 2014b.

Hamid, N. S. A., Gopir, G., Ismail, M., Misran, N., Hasbi, A. M., Usang, M. D., and Yumoto, K.: The Hurst exponents of the geomagnetic horizontal component during quiet and active periods, in: Proc. 2009 Int. Conf. on Space Sci. and Comm., IEEE Publishing, US and Canada, 26–27 October 2009, Port Dickson, Malaysia, 186–189, 2009.

Hargreaves, J. K.: The Upper Atmosphere and Solar-Terrestrial Relations, Van Nostrand Reinhold Co Ltd., Wokingham, England, 298 pp., 1979.

Hargreaves, J. K.: The Solar-Terrestrial Environment, Cambridge University Press, Cambridge, England, 420 pp., 1992.

Hartmann, A., Mukli, P., Nagy, Z., Kocsis, L., and Hermán, P.: Real-time fractal signal processing in the time domain, Physica A, 392, 89–102, 2013.

Heneghan, C., and McDarby, G.: Establishing the relation between detrended fluctuation analysis and power spectral density analysis for stochastic processes, Phys. Rev. E, 62, 6103–6110, 2000.

Hurst, H. E.: Long-term storage of reservoirs: an experimental study, T. Am. Soc. Civ. Eng., 116, 770–799, 1951.

Kantelhardt, J. W., Koscielny-Bunde, E., Rybski, D., Braun, P., Bunde, A., and Havlin, S.: Long-term persistence and multifractality of precipitation and river runoff records, J. Geophys. Res., 111, D01106, doi:10.1029/2005JD005881, 2006.

Kellerman, A. C., Shprits, Y. Y., Makarevitch, R. A., Spanswick, E., Donovan, E., and Reeves, G.: Characterization of the energy-dependent response of riometer absorption, J. Geophys. Res.-Space, 120, 615–631, doi:10.1002/2014JA020027, 2014.

Koscielny-Bunde, E., Bunde, A., Havlin, S., Roman, H. E., Goldreich, Y., and Schnellnhuber, H.-J.: Analysis of daily temperature fluctuations, Phys. Rev. Lett., 81, 729–732, 1998.

Lennartz, S. and Bunde, A.: Trend evaluation in records with long-term memory: application to global warming, Geophys. Res. Lett., 36, L16706, doi:10.1029/2009GL039516, 2009.

Little, C. G. and Leinbach, H.: The riometer – a device for the continuous measurement of ionospheric absorption, P. IRE, 47, 315–320, doi:10.1109/JRPROC.1959.287299, 1959.

Mandelbrot, B. B.: The Fractal Geometry of Nature, W. H. Freeman & Co., New York, 495 pp., 1983.

Mandelbrot, B. B. and van Ness, J. W.: Fractional Brownian motions, fractional noises and applications, SIAM Rev., 10, 422–437, 1968.

Peng, C. K., Mictus, J., Hausdorff, J., Havlin, S., Stanley, H. E., and Goldberger, A. L.: Long-range anticorrelations and non-Gaussian behavior of the heartbeat, Phys. Rev. Lett., 70, 1343–1346, 1993.

Press, W. H. and Rybicki, G. B.: Fast algorithm for spectral analysis of unevenly sampled data, Astron. J., 338, 277–280, 1989.

Rypdal, M. and Rypdal, K.: Stochastic modeling of the AE index and its relation to fluctuations in B_z of the IMF on time scales shorter than substorm duration, J. Geophys. Res., 115, A11216, doi:10.1029/2010JA015463, 2010.

Rypdal, M. and Rypdal, K.: Discerning a linkage between solar wind turbulence and ionospheric dissipation by a method of confined multifractal motions, J. Geophys. Res., 116, A02202, doi:10.1029/2010JA015907, 2011.

Sato, K.: Lévy Processes and Infinitely Divisible Distributions, Cambridge Studies in Advanced Mathematics, 68, Cambridge University Press, Cambridge, 1999.

Wilk, M. B. and Gnanadesikan, R.: Probability plotting methods for the analysis of data, Biometrika, 55, 1–17, 1968.

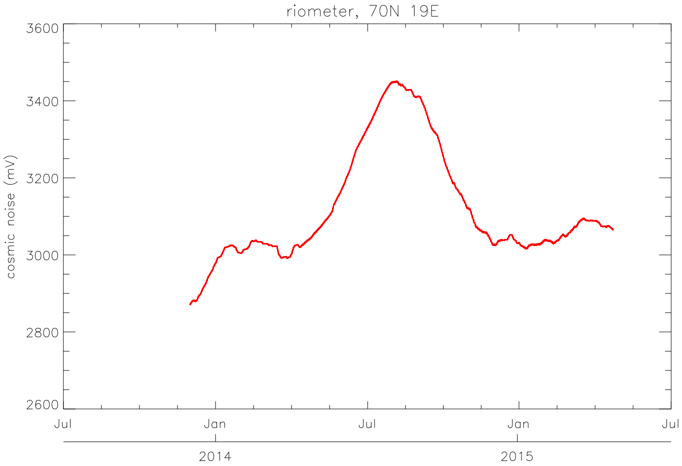

Figure 1. Cosmic noise at 40 MHz measured by riometer at Ny-Ålesund, 79° N, 12° E. Original data at 2 s time resolution have been smoothed by a 1-month boxcar to show both the overall data coverage and seasonal variation.

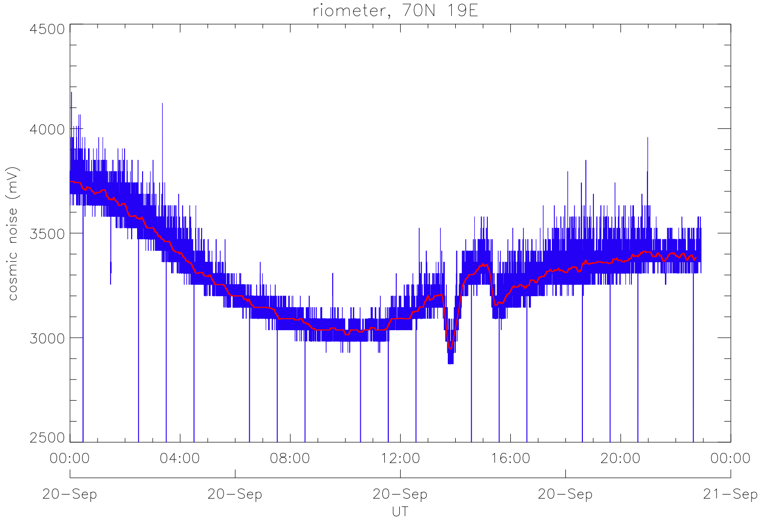

Figure 2. Detail plot of cosmic noise at 40 MHz measured by riometer at Ny-Ålesund, 79° N, 12° E for 20 September 2014. Original samples are shown in the blur curve, which includes the hourly calibration points. A 10 min smoothing is superimposed in red.

Title Page
Abstract
Introduction
Conclusions
References
Tables
Figures
◀◀
▶▶
◀
▶
Back
Close
Full Screen / Esc
Printer-friendly Version
Interactive Discussion

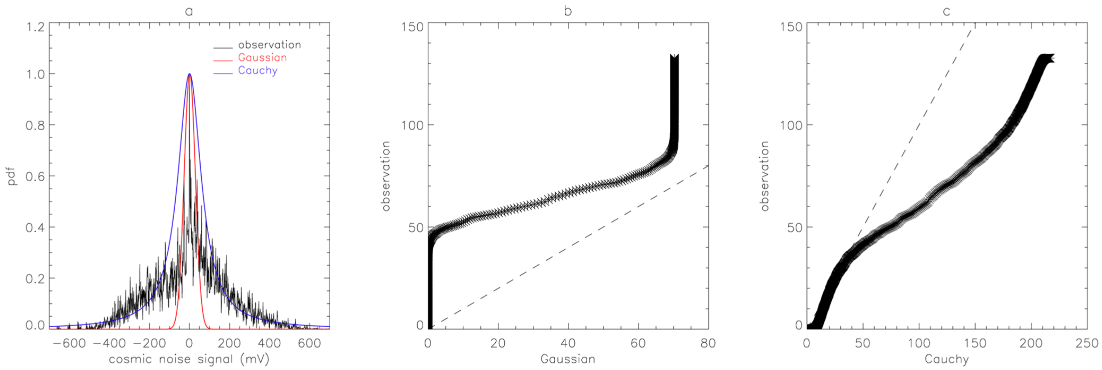

Figure 3. Portrayals of the distribution of the stochastic component (described in the text) of the cosmic noise signal. Left: probability density function with fitted Gaussian (red) and Cauchy (blue) distributions superimposed (explained and discussed in the text). Centre: Q–Q plot of the observed data vs. Gaussian; right: Q–Q plot of the observed data vs. Cauchy.

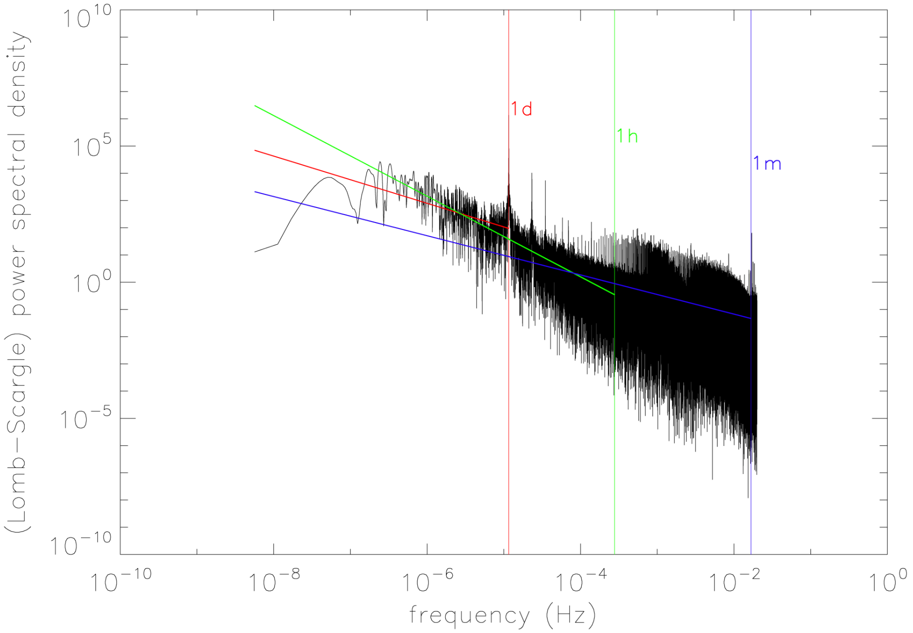

Figure 4. Spectral analysis for data shown in previous figures. Familiar timescales are indicated by vertical dotted/dashed lines. Fitted scaling exponents are shown by coloured lines.